Journal of Power Sources 631 (2025) 236260

Contents lists available at ScienceDirect

Journal of Power Sources

journal homepage: www.elsevier.com/locate/jpowsour

Low nickel loading carbon microfibers fabricated by electrospinning for the glycerol electrooxidation coupled with the continuous gas-phase CO_2 reduction reaction towards formate

Kevin Fernández-Caso [a,1], Zahra Hagheh-Kavousi [b,c,1], Yaovi Holade [b,d], David Cornu [b,d], Guillermo Díaz-Sainz [a,*], Manuel Álvarez-Guerra [a], Angel Irabien [a], Mikhael Bechelany [b,e]

[a] Departamento de Ingenierías Química y Biomolecular, Universidad de Cantabria, Avda. Los Castros, s/n, 39005, Santander, Spain
[b] Institut Europeén des Membranes, IEM-UMR, 5635, ENSCM, CNRS, University of Montpellier, Montpellier, France
[c] Department of Chemistry, Faculty of Sciences, University of Zanjan, P.O. Box: 4537138791, Zanjan, Iran
[d] French Research Network on Hydrogen (FRH2), Research Federation No. 2044 CNRS, BP 32229, Nantes, CEDEX 3 44322, France
[e] Gulf University for Science and Technology, GUST, Kuwait

HIGHLIGHTS

- Nickel carbon microfibers with 5 wt% metal content fabricated via electrospinning.
- Nickel carbon microfibers to catalyze the glycerol electrooxidation reaction.
- MEA electrolyzer for the co-valorization of carbon dioxide and glycerol.
- Continuous gas-phase CO_2 electroreduction to concentrated formate solutions (100 g L^{-1}).
- Simultaneous lactate concentrations of up to 0.114 g L^{-1} in the output anolyte stream.

GRAPHICAL ABSTRACT

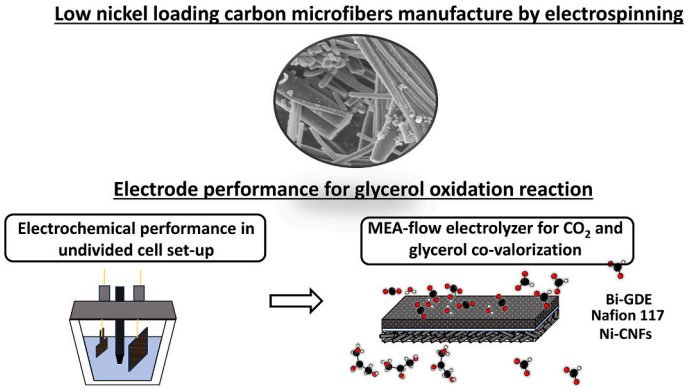

ARTICLE INFO

Keywords:
Single-pass glycerol oxidation reaction
Electrospinning
Nickel carbon microfibers
Gas-phase CO_2 electrolysis
Formate

ABSTRACT

The glycerol market is currently experiencing a surplus due to increased biodiesel production, creating a demand for innovative approaches for its optimal utilization. Electrochemical valorization, particularly electro-oxidation, emerges as a promising solution for transforming excess glycerol into valuable products. Here, we report the use of carbon microfibers with ultralow nickel content (<5 wt %) to catalyze glycerol oxidation reaction (GOR), coupled with continuous gas-phase CO_2 electroreduction to obtain formate. The humidified CO_2-fed membrane electrode assembly electrolyzer, devoid of noble metals, efficiently produces oxidized products like lactate at concentrations of 0.144 g L^{-1} from glycerol and formate solutions reaching up to 100 g L^{-1} from CO_2, surpassing previous methods employing commercial Pt-based materials. This novel approach not only enhances glycerol

* Corresponding author.
E-mail address: diazsg@unican.es (G. Díaz-Sainz).
[1] K. Fernández-Caso and Z. Hagheh-Kavousi contributed equally to this work as co-first authors.

https://doi.org/10.1016/j.jpowsour.2025.236260
Received 26 August 2024; Received in revised form 13 January 2025; Accepted 16 January 2025
Available online 28 January 2025

conversion efficiency but also contributes to sustainable carbon utilization, leading to the production of value-added products.

1. Introduction

Glycerol, a trihydric alcohol, was traditionally considered a critical by-product in the biodiesel and soap manufacturing industries [1]. However, its significance has evolved beyond being a mere waste product [2]. In recent years, glycerol has emerged as a valuable resource with numerous potential applications, owing to its sustainable and renewable origins from triglycerides in vegetable oils and animal fats [3]. This transformation of glycerol from a by-product to a valuable feedstock aligns with the principles of green chemistry and resource efficiency, offering a promising solution to both environmental and economic challenges [3].

The valorization of glycerol involves converting it into valuable products through various chemical, biological, and physical processes [1,4,5]. These routes aim to maximize glycerol utilization while minimizing waste generation, thereby contributing to a more circular and sustainable economy [6,7]. Glycerol valorization can be achieved through several routes. Biological conversion involves using microorganisms and enzymes to ferment glycerol into biofuels, such as ethanol [8] and butanol [9], or valuable chemicals including 1,3-dihydroxyacetone (DHA) [10] and 1,3-propanediol [11]. In chemical transformation, glycerol undergoes catalytic processes to produce compounds such as acrolein [12], glyceric acid (GLYA) [13], and epichlorohydrin [14]. Additionally, thermal conversion methods like pyrolysis [15] and gasification [16] thermally decompose glycerol, yielding syngas, biochar, and intermediate products that can be further processed into chemicals and biofuels. Among various valorization routes, electrochemical oxidation of glycerol stands out as a promising and environmentally friendly approach [17,18]. This method utilizes electrocatalysts to facilitate the controlled oxidation of glycerol at electrode surfaces, offering advantages such as precise control over product selectivity, reduced energy consumption, and minimal waste generation [19,20]. Furthermore, electrochemical oxidation can yield valuable intermediates and fuels with reduced environmental impact, making it a key contender in the quest for sustainable glycerol valorization [17,20]. However, to improve the economic feasibility of the electrochemical valorization pathway, further exploration is needed in the utilization of cost-efficient non-noble metal catalysts [21].

On the other hand, the electrochemical valorization pathway of CO_2 offers the dual benefit of reducing CO_2 emissions, which contribute to climate change, and storing energy from renewable and intermittent sources (e.g., solar and wind energy) in the form of value-added carbon products [22–26]. One of the most promising products generated from CO_2 is formic acid (HCOOH) or formate ($HCOO^-$), which finds applications in several traditional and emergent fields [22,27].

In particular, ongoing operation of electrolyzers fueled by humidified CO_2 has shown great promise in producing HCOOH or $HCOO^-$ [28–32]. These devices not only exhibit noteworthy performance, as indicated by high Faradaic efficiencies and specific energy consumptions for the targeted product, but also result in elevated product concentrations downstream of the electrolyzer [33]. In particular, as can be seen in Table S1 of the Supporting Information, three works develop the continuous gas-phase CO_2 electroreduction to HCOOH by pairing the hydrogen oxidation reaction (HOR) at the anode [31,32,34], and most approaches have been confined to performing the typical OER [28–30,33,35–37]. In this regard, significant efforts are required to integrate more relevant oxidation reactions, such as glycerol oxidation, into the continuous gas-phase CO_2 electroreduction within an membrane electrode assembly (MEA)-reactor, with the aim of enhancing economic feasibility of the whole process [38].

While noble metal catalysts like Pt [39,40], Au [41,42], and Pd [43,44] have traditionally dominated investigations into the GOR, attention is now shifting towards non-noble metal abundant on Earth, such as nickel (Ni), as promising candidates for catalyzing this anodic reaction [45]. In alkaline solutions, Ni readily transforms into $Ni(OH)_2$, where the Ni^{2+}/Ni^{3+} redox centers exhibit notable catalytic efficacy in oxidizing various small organic compounds [46,47]. This makes the use of Ni-based anodes for conducting GOR under alkaline conditions, alongside emerging processes like CO_2 reduction, a highly favourable option for co-valorization.

Recent efforts have focused on coupling GOR with continuous CO_2 reduction reactions to produce value-added chemicals, such as carbon monoxide (CO) [48–51] or ethylene (C_2H_4) [52] and particularly $HCOO^-$ [53–60], with only three approaches successfully achieving this coupling by Ni-based anodes with high metal deposition rates [58–60]. Junqueira et al. [58] engineered a 0.95 cm^2 flow cell, facilitating CO_2 reduction to $HCOO^-$ at the bismuth gas diffusion electrode (Bi-GDE), while the GOR predominantly occurred at the surface of the NiB_x/Ni foam anode, resulting mainly in $HCOO^-$ as the product. Van den Bosch et al. [59] adopted a strategy using a Ni_3S_2/Ni foam anode to catalyze the GOR towards $HCOO^-$ formation, while the concurrent CO_2 reduction towards $HCOO^-$ was achieved at the InBi-GDE. Finally, in our recent study, we designed a MEA-reactor to enable the gas-phase CO_2 reduction to $HCOO^-$ at the Bi-GDE in continuous mode. Simultaneously, single-pass GOR occurred at the Ni-Co/Ni foam anode surface, yielding $HCOO^-$ and other high-value products, such as DHA [60].

Although the Ni-based anodes utilized in the studies [58–60] demonstrate compelling performance regarding wettability and mass transport properties [60–64], their usage involves high rates of metal catalyst deposition. Given that nickel is classified as a critical raw material by the European Union and the United States, signifying its essential role in their economies and the high risk associated with its supply disruption, it is vital to minimize metal loadings to reduce costs and ensure the sustainable development of such devices. For this purpose, several methods exist for preparing catalysts with reduced metal content, with electrospinning (ES) emerging as a particularly intriguing approach to produce homogeneously distributed metal-coated carbon microfibers (CMFs) [65–67]. Unlike methods involving Ni foam substrates with high Ni metal loading deposition rates, ES offers the potential to create ultra-low metal loading anodes, facilitating efficient catalysis of the GOR [44,68]. Furthermore, CMFs structures exhibit enhanced performances in terms of conductivity and thermal, mechanical stability [67,69,70], in addition to having a micropore-free graphite structure and being cost-effective [66,69,71].

Here, we report the utilization of nickel nanoparticles supported on CMFs (Ni-CMFs) with ultra-low Ni content (<5 wt %) as a promising material to catalyze the GOR. Furthermore, the Ni-CMFs were used as anode catalysts in a MEA-electrolyzer to facilitate the single-pass GOR towards different products, while the continuous gas-phase CO_2 reduction reaction towards concentrated $HCOO^-$ solutions takes place on the surface of the Bi-GDE. This approach offers a feasible method to co-valorize CO_2 and glycerol without the need for noble catalytic metals to produce value-added products in both compartments of the electrochemical reactors.

2. Methodology

2.1. Materials

Polyacrylonitrile (PAN, Mwt ~ 150 000, CAS 25014-41-9, Sigma-Aldrich), nickel (II) chloride, ($NiCl_2$, 98 %, CAS no. 7718-54-9, Sigma-Aldrich), N,N-dimethylformamide (DMF, 98 %, CAS no. 68-12-2,

Sigma-Aldrich) and ethanol (C_2H_5OH, 99 %, CAS n°. 64-17-5, Sigma-Aldrich) were used to fabricate free-standing Ni-CMF electrodes through ES. Potassium hydroxide (KOH, CAS 1310-58-3, Sigma-Aldrich) was used as an electrolyte solution. Glycerol (Glycerol, 99 % purity, ReagentPlus, Sigma Aldrich) was used to prepare the electrolyte. DHA (CAS n°. 96-26-4, Sigma-Aldrich), glyceraldehyde (GLAD) (CAS n°. 56-82-6, ≥98 % (HPLC), Sigma Aldrich), HCO_2Na in H_2O (Ion chromatography standard solution, 1000 μg L^{-1}, Thermo Scientific), lactic acid (CAS n°. 50-21-5, Sigma Aldrich), glycolic acid (CAS n°. 79-14-1, Sigma Aldrich) and Calcium DL-glycerate dihydrate ($C_6H_{10}CaO_8{\cdot}2H_2O$, CAS n°. 67525-74-0, Thermo Scientific) were used as reactants to prepare standard solutions for high performance liquid and ionic chromatography. Sulfuric acid (H_2SO_4, CAS no. 7664-93-9, 97 %, Sigma-Aldrich) was employed to neutralize the measured sample for the detection of GLAD and DHA. A commercial carbon paper substrate (AvCarb MGL190, Fuel Cell Store (USA)) and a commercial carbon paper with a microporous layer (MPL) (Sigracet 28 BC, Fuel Cell Store (USA)) were used as supports for Ni-CMF in static measurements within a three-electrode cell and an H-type cell, respectively. A commercial platinum gauze (52 mesh, dimensions 25 × 25 mm) was utilized as the counter electrode during bulk electrolysis in the H-cell configuration. The H-type cell was separated by a hydroxide anion exchange membrane (AEM), Sustainion® X37-50 Grade RT (50 μm dry thickness) procured from Fuel Cell Store (USA). The membrane underwent activation in 1 M KOH for 24 h at 22 ± 3 °C and was subsequently rinsed abundantly with Milli-Q water. A commercial carbonaceous substrate (Teflonated Toray carbon paper TGP-H-60) was employed as support for the Bi-GDE. Carbon cloth (FuelCell, CeTech Carbon Cloth without MPL – W0S1011) was used as Ni-CMFs substrate for the MEA-flow reactor tests. Black carbon (Vulcan X-72R) and PTFE (Polytetrafluoroethylene preparation, 60 wt % dispersion on H_2O, Sigma Aldrich) were engaged for the preparation the MPL of the Bi-GDE. Carbon-supported bismuth nanoparticles (whose synthesis and characterization are reported in previous works (Fig. S1 of the Supporting Information) [33,72]) as cathode catalyst for the selective CO_2 reduction toward $HCOO^-$ and Nafion-ionomer (Nafion D-521 dispersion, 5 w/w % in water and 1-propanol, 0.92 meq g^{-1} exchange capacity) were used to prepare the catalytic layer of the Bi-GDE. A Nafion 117 cationic exchange membrane (Alfa Aesar) was employed as compartment separator of the MEA-flow reactor.

2.2. Nickel carbon microfibers manufacture

The production process of Ni-CMFs mats involved a structured three-step process, comprising (i) electrospinning, (ii) thermal oxidation, and (iii) thermal pyrolysis [66]. In a concise overview, a solution was created by dissolving PAN/$NiCl_2$ (as the metal precursor)/DMF in 18 mL of solvent. PAN powder was subsequently added to the solution, which was continuously stirred for 24 h to ensure a uniform mixture. For the electrospinning phase, solutions containing less than 5 wt % of the metal precursor were loaded into 15 mL plastic syringes. Electrospinning was carried out under specific conditions, including a tip-to-collector distance of 15 cm, an operating voltage of 19 kV, a flow rate of 3 mL h^{-1}, and a drum rotating speed of 2000 rpm (Fig. S2 of the Supporting Information).

Following electrospinning, the microfiber mats underwent thermal oxidation for a duration of 2 h at 235 °C. Subsequently, thermal pyrolysis was conducted for 1 h under a nitrogen (N_2) atmosphere at a consistent heating and cooling rate of 5 °C min^{-1}, reaching a temperature of 1200 °C.

2.3. Physico-chemical characterization of nickel carbon microfibers

X-ray Diffraction (XRD) determined crystal structure and crystallite size using a Bruker D8 Discover diffractometer, features a Johansson monochromatic optimized for CuKα$_1$ radiation and is equipped with a LynxEye XE-T detector. This diffractometer, set at 40 kV and 40 mA, produced diffraction patterns ranging from 10° to 90°, at a scan rate of 3.6° per minute and a step size of 0.025°. Microscopy techniques, including Scanning Electron Microscopy (SEM, Hitachi S4800 microscope) with an energy dispersive X-ray (EDS) analysis (ZEISS EVOHD 15 microscope) and High-Resolution Transmission Electron Microscopy (HRTEM, FEG JEOL 2200FS microscope (200 kV)), explored physical attributes such as fiber diameter, surface morphology, composition, and crystallinity. X-ray photoelectron spectroscopy (XPS) using a Thermo Electron ESCALAB 250 spectrometer, operating at Al Kα radiation (1486.6 eV, 15 kV, 6 mA) as an excitation source, determined elemental composition and chemical states. The thermogravimetric analysis (TGA) was carried out using the SDT simultaneous Q600 from TA Instruments, which couples ATG-DSC.

2.4. Electrochemical characterization of nickel carbon microfibers-based electrodes

The preparation of catalytic ink for Ni-CMFs follows standard procedures. Initially, a slurry containing 5 mg of Ni-CMFs, 100 μL of Nafion ionomer (Nafion D-521 dispersion), and 2 mL of ethanol is ultrasonically mixed to ensure homogeneity. Subsequently, 250 μL of this homogeneous ink is drop-cast onto each face of a bare L-shaped CP electrode (to achieve a catalyst loading of 0.59 mg cm^{-2} on both sides of the carbon substrate), measuring 1 cm in height and 1 cm in width, and then allowed to dry at room temperature. Once dry, the electrode serves as the working electrode for electrochemical measurements.

Electrochemical characterizations were conducted using a SP-150 potentiostat from Biologic Science Instruments. The electrocatalytic performance of Ni-CMFs electrodes was assessed in a conventional three-electrode, single compartment cell, maintained at a constant 25 °C. The setup included a mercury-mercury oxide (Hg|HgO| 1.0 M KOH) electrode (MOE, RE-61AP, BAS Inc.) as the reference, calibrated against a Reversible Hydrogen Electrode (RHE) using ($E_{(RHE)} = E_{(MOE)} + 0.92$) formula; a glassy carbon plate (12.4 cm^2) as the counter electrode. Experiments were conducted in a 1 M KOH solution saturated with Ar, in the presence of 0.1 M glycerol for GOR.

To activate and stabilize the electrodes, cyclic voltammetry (CV) was performed for 10 cycles at a constant scan rate of 100 mV s^{-1}. Moreover, electrochemical impedance spectroscopy (EIS) was conducted over a frequency range spanning from 10^{-3} to 200 kHz at different applied working potentials of 1.2, 1.25, 1.3, 1.35 and 1.4 V vs. RHE (potential higher than onset potential value for GOR). By last, chronoamperometry (CA) measurements were carried out at applied working potential of 1.265 V vs. RHE for 1 h.

2.5. Humidified CO_2-fed MEA-reactor and analytical techniques

All tests in flow conditions were carried in a MEA-reactor (Electro-Cell A/S, depicted in Fig. S3 of the Supporting Information with its different stacked components), in which a humidified CO_2 stream was fed in the cathode compartment. The vapour mixture consisted of a pure CO_2 flow rate of 200 mL_n min^{-1} with 2 g h^{-1} of water steam (equivalent to 0.02 molH_2O [mol CO_2 cm^2]$^{-1}$) mixed in the Coriolis flowmeter of the Vapour Delivery Module (Vapour Delivery Module, Bronkhorst). This water flow rate in the CO_2 stream was selected as the reference operating condition based on previous studies we conducted on the influence of this variable [33]. Fig. 1 shows the experimental set-up employed to study the continuous co-valorization of CO_2 and glycerol with Ni-CMF-based electrodes. The anolyte composition was 1.0 M KOH +1.0 M glycerol to compare the results with our previous works with the same electrochemical device and operating conditions [33,60]. Additional digital images of the experimental set-up employed are included in Fig. S4 of the Supporting Information.

The anode, as the main novelty of this work, was prepared by air-brushing the above prepared Ni-CMF onto a carbon cloth support for tests in the MEA-flow cell in galvanostatic conditions. For this last case,

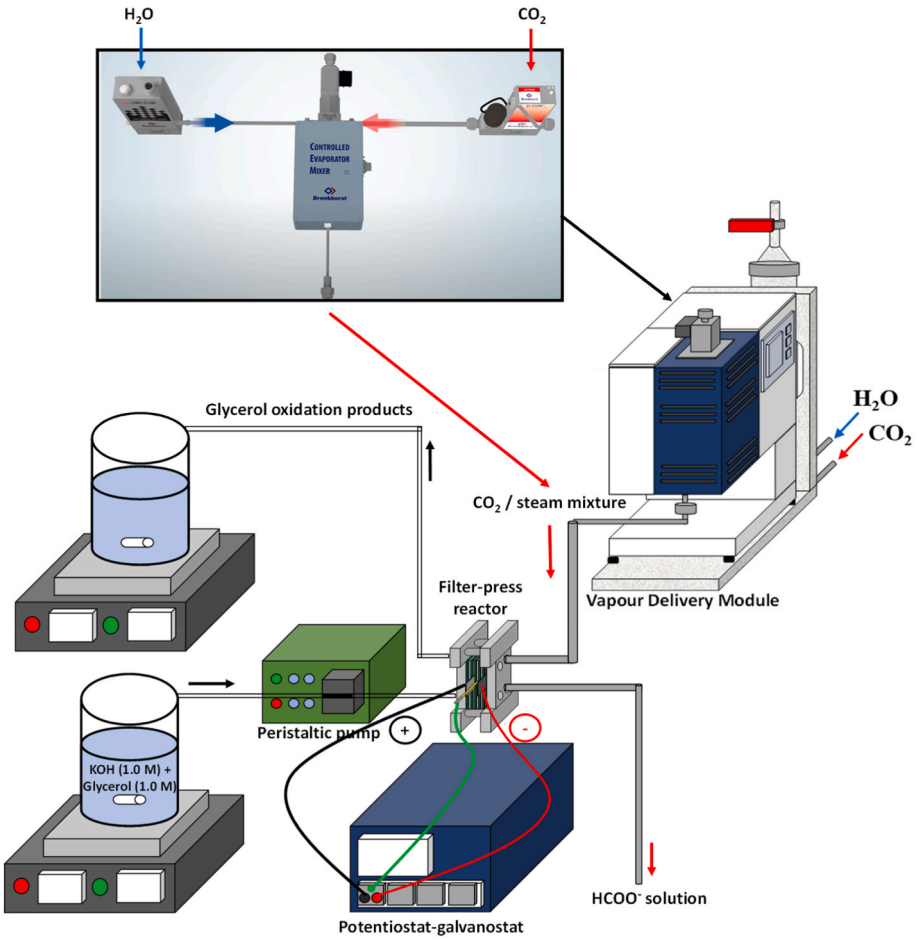

Fig. 1. The experimental configuration involved the introduction of an aqueous anolyte (1.0 M KOH + 1.0 M glycerol) to the anode side and a CO_2/steam mixture to the cathode side of the constructed electrolyzer featuring Ni-CMFs-anodes.

the anode comprises a highly conductive and hydrophilic carbonaceous substrate, onto which the as-prepared Ni-CMF were deposited with Nafion-ionomer in a 70/30 wt % ratio, respectively. This Ni-CMF/Nafion-ionomer mixture was in turn diluted in isopropanol 3 wt % and then sonicated in ultrasounds for 1 h, and then deposited over the carbon cloth substrate by air-brushing technique, forming the Ni-CMF-based anode (with Ni-CMF loading of 1.00 mg cm^{-2}).

The procedure for the fabrication of Bi-GDE as well as its characterization is detailed in previous works (Fig. S5 of the Supporting Information) [33,72]. A cationic exchange membrane (Nafion 117), previously activated in a 1.0 M KOH solution for at least 1 h, was employed as compartment separator to prevent product crossover. This is crucial since a significant portion of the products formed in the alkaline environments of both the cathode ($HCOO^-$) and anode ($HCOO^-$, LAC, GLYA, among others) are anions. The geometric surface area of both anode and cathode (Ni-CMF-based anode and Bi-GDE) in the humidified CO_2-fed MEA electrolyzer was 10 cm^2.

The $HCOO^-$ concentration in both the cathodic output stream and anolyte was determined using ion chromatography with a Dionex ICS system equipped with an AS9 – HC column. The eluent employed was Na_2CO_3, with specific parameters including a concentration of 4.5 mM, a flow rate of 1 mL min^{-1}, a conductivity of 15 μS, and a pressure of 1800 psi.

For the detection and quantification of glycerol oxidation products (DHA, GLAD, lactate (LAC), GLYA, and glycolate (GLYC)) a High-Performance Liquid Chromatography (HPLC) equipment was employed. The system comprised an Agilent 1100 series VWD with a diode detector (Agilent 1260 Infinity II at different wavelenghts of 210, 254 and 271 nm) and an ion exchange column (Hi-Plex-H, 300 × 7.7 mm, Agilent). The eluent composition consisted of a 5 mM H_2SO_4 aqueous phase and an organic phase of Acetonitrile (Acetonitrile CHROMASOLV™ Plus, for HPLC ≥99.9 %) in a volumetric ratio of 94/6 v/v %. HPLC conditions included a constant flow rate of 0.6 mL·min^{-1}, a column temperature set at 50 °C, and a fixed injection volume of 50 μL for all samples.

The procedure for the calculation of the figures of the cathode and anode can be found in Equations S1-S11 of the Supporting Information.

3. Results and discussion

3.1. Physico-chemical characterization of nickel carbon microfibers

The SEM image in Fig. 2a reveals the relatively uniform dispersion Ni nanoparticles with low content across the CMFs. Additional characterization information based on back-scattered electrons field emission SEM/EDS mapping of Ni-CMFs can be found in Figure S6, Table S2 and Table S3 of the Supporting Information. The EDS spectrum of various sections of the Ni-CMFs sample particularly reveals a nickel content of 3.9 wt %, equivalent to a nickel loading per geometric anode surface area of less than 50 μg cm^{-2} (Table S3). TGA curve presented a shoulder just before the start of the sharp loss in weight, indicating the presence of CMFs (Figure S7 of the Supporting Information). More in-depth studies with TEM and HRTEM of interfaces have also been performed on Ni-CMFs, and the images obtained clearly reveal that consist of nickel nanoparticles encapsulated by multiple layers of stacked carbon or graphene (Fig. 2b). Furthermore, TEM/EDS mapping (Figure S8 of the

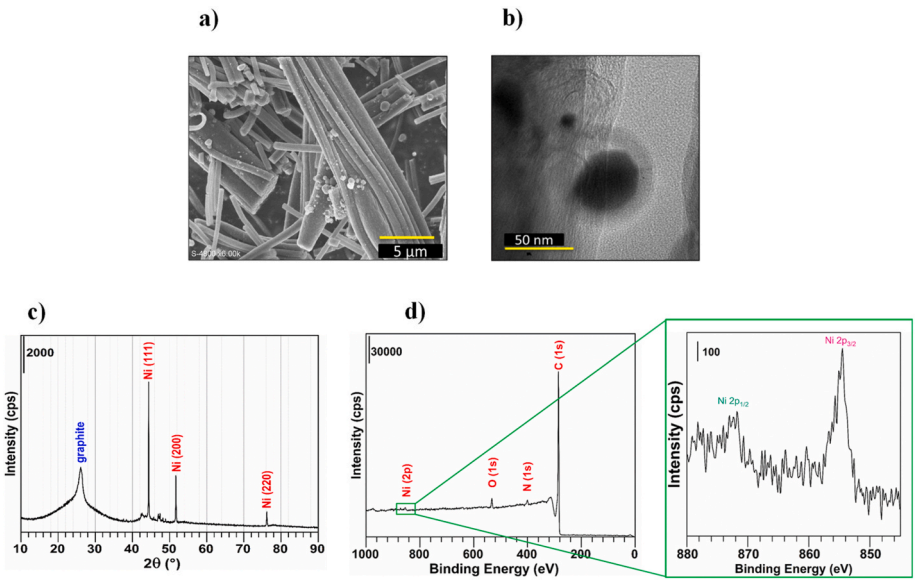

Fig. 2. **a)** Field-emission SEM image, **b)** TEM analysis, **c)** XRD patterns and **d)** representative XPS survey scan of Ni-CMFs.

Supporting Information) shows the presence and homogeneity of Ni nanoparticles on the surface of microfibers. However, HRTEM images indicate a wide and random size distribution of nickel particles, ranging from 8 to 78 nm. This variability in particle size is likely a result of the inherent inconsistencies in the electrospinning and thermal treatment processes, which lead to uneven nucleation and growth during pyrolysis. Next, XRD measurements used to determine the crystallographic structure of the Ni-CMFs. As shown in Fig. 2c, a peak at 26° is indicative of graphite, while peaks at 44.4, 51.7, and 76.3° correspond to the (111), (200), and (220) crystallographic orientations of nickel, respectively (JCPDS: 96-210-2279) [73,74], confirming the presence of Ni in the Ni (0) state. XPS analysis performed to obtain in-depth knowledge about compositional features of the Ni–CMFs, and surface state. The survey XPS spectra shown in Fig. 2d reveal distinct features of the of Ni 2p (binding energy of 854.5 eV), O 1s (binding energy of 532.65 eV), N 1s (binding energy of 400.9 eV) and C 1s (binding energy of 284.8 eV) for Ni–CMFs. Additional XPS details for C, O, and N are provided in Figure S9. Notably, the peak for Ni 2p appears with less intensity compared to the other two peaks (Ni $2p_{3/2}$ at 854.5 eV and Ni $2p_{1/2}$ at 871.8 eV), which may suggest a low nickel loading or a more dispersed

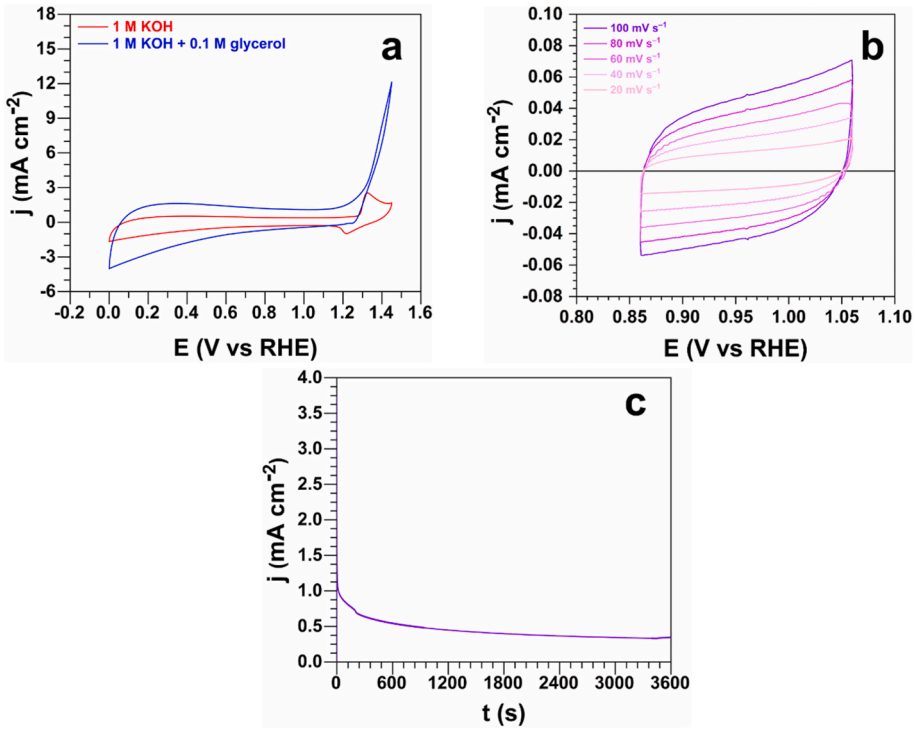

Fig. 3. **a)** CV of Ni-CMF (0.5 mg cm^{-2}) measured in absence (blue line) or presence of 0.1 M glycerol (red line) (50 mV s^{-1}, 1 M KOH, 25 °C). **b)** Electrochemical double-layer capacitance measurement with the CV curves acquired at different scan rates from 20, 40, 60, 80, and 100 mVs^{-1} in 1 M KOH at 25 °C. **c)** CA measurement at $E_{appl.}$ = 1.265 V vs. RHE in 1 M KOH +0.1 M glycerol at 25 °C. (For interpretation of the references to colour in this figure legend, the reader is referred to the Web version of this article.)

distribution on the microfibers. This low intensity contributes to a high signal-to-noise ratio, making high-resolution decomposition of the Ni 2p peaks challenging and leading to larger margins of error. More information about XPS spectra of Ni-CMFs is available in the Table S4 of the Supporting Information.

3.2. Electrochemical characterization of nickel carbon microfibers

The CV profile of Ni-CMFs in 1 M KOH (Fig. 3a with a blue line) elucidates the electrochemical characteristics of Ni in an alkaline electrolyte, delineating three main potential regions [75,76]. The first region, ranging from 0.7 to 1.0 V vs. RHE, corresponds to the double-layer formation. The second, from 1.1 to 1.3 V vs. RHE, is characterized by the coverage of the electrode by nickel hydroxides. The third region, from 1.3 to 1.4 V vs. RHE, involves the redox couple of Ni^{2+}/Ni^{3+}. The electrocatalytic activity of catalysts correlates with the electrochemical active surface area (ECASA = C_{dl}/C_s, C_s = reference capacitance of the monolayer, which value depends on the nature of the electrode material). A larger ECASA suggests more active sites and consequently, improved catalytic activity. To evaluate ECASA, we measured the electrochemical double-layer capacitances (C_{dl}) in the non-Faradaic region where there is no current by adjusting the working potential (from 0.86 to 1.06 V vs. RHE) at different scan rates (20, 40, 60, 80 and 100 mV s^{-1}) using CV (Fig. 3b). As shown in Fig. S10 of the Supporting Information, depicting current values against the different scan rates (0.02–0.1 V s^{-1}), a fitted capacitance value of 0.84 mF was obtained for Ni-CMFs. The low Ni metal content observed in SEM and EDS mapping (Fig. S6, Tables S2 and S3 of Supporting Information) confirms the low fitted capacitance value of Ni-CMF However, the estimated C_{dl} via CV differs from the value determined through EIS (Table S5). This difference is expected, as the EIS measurements were conducted in the presence of glycerol and under reaction conditions where the applied potential was not within the non-Faradaic region. Therefore, the C_{dl} estimation from EIS reflects the electrochemical environment during the reaction, while the CV-based C_{dl} measurement represents the non-Faradaic double-layer capacitance under different experimental conditions.

When the electrolyte contains 0.1 M glycerol, the onset potential for glycerol oxidation with Ni-CMF is observed only in the higher potential range, occurring at ca. 1.1 V vs. RHE (Fig. 3a with a blue line). This potential also marks the beginning of NiOOH formation. Therefore, on nickel, the GOR is facilitated by the $Ni(OH)_2$/NiOOH film [77,78]. EIS was utilized to examine the rate of charge transfer at the electrode/electrolyte interface. The Nyquist impedance plot and the data underwent fitting utilizing the representative equivalent electrical circuit (EEC) comprising $R_\Omega + Q_{CPE}/R_{ct}$ (Fig. S11 and Table S6 of the Supporting Information). CA measurements (Fig. 3c) carried out for 3600 s elucidated that for working potentials of up 1.265 V vs. RHE (higher than the onset of 1.1 V vs. RHE), the current was held constant at an average value of 0.4–0.5 mA cm^{-2}.

Chronopotentiometry (CP) analysis was performed to evaluate the stability of the Ni-CMF electrode during prolonged electrochemical operation (Fig. S12) using an H-type cell to precisely control the reaction environment in the anodic compartment. The experiment was conducted at an applied current density of 45 mA cm^{-2}, with the GOR occurring in the anodic compartment and the hydrogen evolution reaction (HER) on a platinum counter electrode in the cathodic compartment. A stir bar was employed to enhance mixing and mitigate mass transport limitations in the electrolyte. Despite these measures, significant potential fluctuations were observed after approximately 1 h of operation and persisted throughout the experiment. These fluctuations were primarily attributed to dynamic changes at the anodic Ni-CMF electrode. Surface transformations, including the formation and reduction of nickel oxides or hydroxides, likely induced intermittent variations in catalytic activity. Additionally, the porous structure of the Ni-CMF electrode may have contributed to localized mass transport limitations, where reactant depletion or product accumulation within the pores resulted in uneven current distribution, further exacerbating potential instability. Post-mortem SEM imaging and elemental mapping (Figs. S13 and S14) were performed to assess the structural and compositional integrity of the Ni-CMF electrode before and after the reaction. SEM images revealed that the distribution of nickel species on the CMF surface and the overall morphology of the electrode remained unchanged after the reaction, with no significant aggregation or structural anomalies observed. Elemental mapping (Fig. S14) further confirmed consistent spatial distribution of nickel, oxygen, and carbon before and after the reaction. These findings suggest that, while dynamic surface transformations occurred during operation, the electrode maintained its structural integrity and active material distribution, demonstrating stability under electrochemical conditions.

3.3. Test in a flow reactor paired with the CO_2 reduction on Bi-GDE

3.3.1. Ni-CMF-based anode performance for the single-pass GOR

All experiments were conducted at fixed H_2O/CO_2 molar ratio per geometric surface area (Vc/A) and current density (j) of 0.02 molH_2O [molCO_2 cm^2]$^{-1}$ and 45 mA cm^{-2}, respectively, to assess the effect of anolyte flow rate per geometric surface area (Qa/A) on the glycerol oxidation product distribution. To facilitate the observation of the main trends in the product distribution from GOR at the anode, Fig. 4 depicts the product concentrations (Fig. 4a) and their Faradaic efficiencies (Fig. 4b) against the Qa/A. In the initial experiments, feeding an Qa/A of 0.57 mL min^{-1} cm^{-2} revealed that the main products formed from GOR were $HCOO^-$ and LAC with concentrations of up to 212.8 mg L^{-1} and 195.89 mg L^{-1}, respectively (Fig. 4a). Additionally, another C3 product from GLAD oxidation, such as GLYA, was detected in concentrations of 64.23 mg L^{-1} (Fig. 4a), resulting in Faradaic efficiencies for this product of 4.92 % (Fig. 4b). Trace amounts of intermediates such as GLAD (3.56 mg L^{-1}) and DHA (1.95 mg L^{-1}), as well as C2-product such as GLYC with concentrations of only 2.40 mg L^{-1}, were also measured (Table S7 of the Supporting Information). Considering the above concentrations of $HCOO^-$ and the Qa/A (0.57 mL min^{-1} cm^{-2}) pumped into the MEA-reactor, production rates and Faradaic efficiencies for $HCOO^-$ of 449.25 μmol m^{-2} s^{-1} (Figure S15 of the Supporting Information) and 25.68 % were obtained, respectively, showing the intrinsic preference of Ni-based materials towards this C1-products [58,59]. The presence of DHA is correlated with the Faradaic efficiencies for LAC (8.85 %), since LAC is the main by-product from DHA degradation (not through the electrochemical oxidation route) in highly alkaline environments (pH 14) [55].

By increasing the Qa/A from 0.57 to 2.28 mL min^{-1} cm^{-2}, the concentrations of oxidized products decreased due to product dilution (Fig. 4a). Surprisingly, LAC was the main C3-product from GOR, with interesting concentrations of up to 114 mg L^{-1} (a reduction of almost 72 % compared to the value obtained at Qa/A of 0.57 mL min^{-1} cm^{-2}, Fig. 4a), and DHA was not detected in the HPLC. Consequently, Faradaic efficiencies for LAC increased from 8.85 to 20.68 %. GLYA was also measured with low concentrations of up to 18.75 mg L^{-1}, which, combined with high Qa/A of 2.28 mL min^{-1} cm^{-2}, led to increase the Faradaic efficiency towards this product of almost 17 % (from 4.92 to 5.75 %, Fig. 4b). Nevertheless, the main oxidized product from GOR under these anode conditions was again $HCOO^-$, with concentrations of almost 80 mg L^{-1} (representing a reduction of up to 62 %) measured in the output anolyte stream, assuming an increase in the production rate and Faradaic efficiency towards this product of up to 50 % (Fig. 4 and Fig. S15 of the Supporting Information). Despite requiring a significantly smaller amount of active metal catalyst (0.05 mg cm^{-2}) compared to Ni-Co/Ni foam electrodes (8.00 mg cm^{-2}) [79], the anode potentials of the current Ni-CMF-based electrodes (ranging from 2.49 to 2.68 V vs. Ag/AgCl) closely approximate those achieved by Ni-Co/Ni foams (ranging from 2.29 to 2.39 V vs. Ag/AgCl). While Ni catalysts are renowned for their high selectivity in generating C1 products such as

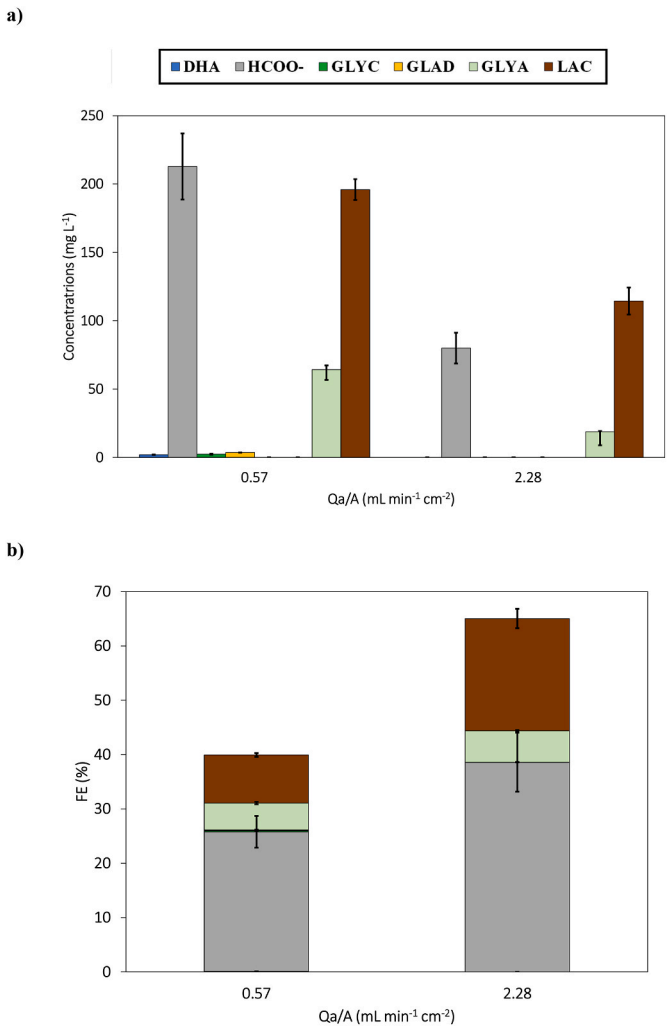

Fig. 4. a) Glycerol oxidation products concentrations measured in the output anolyte stream and **b)** their Faradaic efficiencies for the experiments in the gas-fed MEA reactor system as function of the anolyte flow rate per geometric anode surface area [Qa/A] pumped to the humidified CO_2-fed MEA electrolyzer developed in this work for a fixed current density [j] of 45 mA cm^{-2}.

$HCOO^-$ from glycerol, the combined use of a single-pass anolyte operation through the MEA-reactor with the relatively low anode overpotentials observed, facilitates the production of less oxidized products like LAC and GLYA with notable efficiency. The proposed reaction pathways are summarized in Scheme S1. The GOR pathway over Ni-CMFs involves stepwise oxidation of glycerol to intermediates like GLAD and DHA, leading to final products such as GLYA, LAC, and $HCOO^-$. CV results indicate that the GOR is closely tied to the Ni $(OH)_2$/NiOOH redox couple, with oxidation initiating at potentials exceeding 1.1 V vs. RHE, where NiOOH formation begins (Fig. 3a) [80]. These findings explain the selective production of C1 ($HCOO^-$) and C3 (LAC, GLYA) products.

3.3.2. *Cathode performance for $HCOO^-$ production from CO_2*

The initial experiments with Ni-CMF were carried out at Vc/A, j and Qa/A of 0.02 molH_2O [molCO_2 cm^2]$^{-1}$, 45 mA cm^{-2} and 0.57 mL min^{-1} cm^{-2}, respectively. Under these operating conditions, $HCOO^-$ concentrations of 74.8 g L^{-1} were achieved in the cathodic compartment of the electrolyzer, along with acceptable Faradaic efficiencies for this product of 63.4 %. During these duplicated tests with Ni-CMF anodes, an average absolute cell voltage of 3.59 V was reported, resulting in specific energy consumptions of 305 kWh $kmol^{-1}$. As illustrated in Table 1, a significant portion of the cell voltage is attributed to the anode potential (2.49 V vs. Ag/AgCl). This value closely aligns with that achieved by Ni-Co/Ni foam (2.29 vs. Ag/AgCl) [60], despite the lower metal loading of Ni-CMFs compared to the high metal deposition rate of Ni-Co/Ni foam [60,79]. Even though the implementation of a particulate Pt electrode as the anode (Pt/C-PE) for GOR at a Qa/A of 0.57 mL min^{-1} cm^{-2} enhances the formation of more concentrated $HCOO^-$ solutions (89.5 g L^{-1}) at the cathode side compared to the system developed in this work (74.8 g L^{-1}), the absolute voltages registered with Pt/C-PE were almost 40 % higher than those obtained with Ni-CMF anode, resulting in a significant improvement in terms of energy consumptions (from to 467 to 305 kWh $kmol^{-1}$).

By increasing the Qa/A from 0.57 to 2.28 mL min^{-1} cm^{-2}, a notable effect in the formation of $HCOO^-$ from CO_2 can be observed with implementation Ni-CMF as the anode, resulting in enhancements in $HCOO^-$ concentration and related figures of merit (Table 1). This trend was also observed in our previous work with Ni-Co/Ni foam [60], and it may be attributed to an optimized balance between membrane hydration and potassium (K^+) availability near the catalyst surface. This equilibrium is crucial for the formation of reduced CO_2 products [81], facilitating the collection of concentrated $HCOO^-$ directly from the cathodic stream [30,60]. By employing Ni-CMF-based anodes and adjusting the Qa/A from 0.57 to 2.28 mL min^{-1} cm^{-2}), the concentration of $HCOO^-$ increased from 74.8 to 100.1 g L^{-1}, as shown in Table 1. Consequently, Faradaic efficiencies saw a 15 % improvement due to major cathodic $HCOO^-$ productions under these conditions. Despite a slight nearly 2 % increase in absolute cell voltages (from 3.59 to 3.66 V), energy consumption per kmol of $HCOO^-$ showed a reduction of almost 12 % (from 305 to 269 kWh $kmol^{-1}$). Under these operating conditions with Ni-CMF-based anodes, the cathode performances surpassed those achieved by Pt/C-PE, yielding almost 23 % higher $HCOO^-$ concentrations and improved Faradaic efficiencies towards this product of up to 72.9 % (compared to Faradaic efficiencies for $HCOO^-$ of 39.9 % obtained with Pt/C-PE). It is evident once again that the higher absolute cell voltages measured with Pt/C-PE (5.06 V), resulted in worsened energy consumptions (700 kWh $kmol^{-1}$) compared to the values obtained with Ni-CMF-based anodes (269 kwh·$kmol^{-1}$). In this context, the humidified CO_2-fed MEA electrolyzer developed in this study demonstrates compelling performance in generating concentrated $HCOO^-$ solutions from CO_2 at the cathode, surpassing our previous work with noble metal-based anodes such as Pt. This underscores the feasibility of the integrated electrochemical device, enabling the seamless coupling of continuous gas-phase CO_2 electroreduction with the GOR catalyzed by Ni-CMF-based anode.

4. Conclusions and future perspectives

This study focuses on the fabrication and characterization of Ni-CMFs with ultra-low Ni content (<5 wt %) for catalyzing the GOR. This material exhibits interesting performances by preventing the agglomeration of unsupported Ni nanoparticles.

On one hand, ECASA measurements in 1.0 M KOH indicate that Ni-CMF catalysts have low fitted capacitance values of 0.85 mF (contrasting the information revealed by EDS mapping). On the other hand, the electrochemical characterization in 1.0 KOH +0.1 M KOH shows that GOR occurs at higher anode potentials of 1.1 V vs. RHE with Ni-CMF. Most of the bibliography reports that under these potentials, Ni-based electrocatalysts have low selectivity towards C3-products, mainly producing C1-products such as $HCOO^-$ from glycerol. Previous methodologies [55,57,60] have demonstrated that utilizing flow reactors with single-pass reactants through the cell enables the alteration of product distribution. This is achieved by adjusting the residence time of oxidized glycerol products through the manipulation of the anolyte flow rate. This modification influences the re-oxidation pathways or degradation

Table 1
Bi/C-GDE (with catalyst loading of 1.50 mg cm^{-2}) performance in the $HCOO^-$ production in the gas-fed MEA reactor system for continuous CO_2 and glycerol co-valorization by working with at a H_2O/CO_2 molar ratio per geometric surface area and a current density of 0.02 $molH_2O$ [$molCO_2$ cm^2]$^{-1}$ and 45 mA cm^{-2}, respectively, taking into account **(i)** the counter electrode and the oxidation reaction of the anode which can be glycerol (GOR) which can be catalyzed by the Pt/C-PE, Ni-Co/Ni foam-based anodes [60] or the as-prepared Ni-CMF-based electrodes for this work; or water oxidation (OER) boosted by DSA/O_2 [33]; **(ii)** the anolyte flow rate per geometric anode surface area [Qa/A]; **(iii)** the absolute cell voltage; **(iv)** the anode potential; **(v)** the $HCOO^-$ concentration [$HCOO^-$]; **(vi)** the Faradaic efficiency [FE] towards $HCOO^-$; **(vii)** the production rate of $HCOO^-$ [r$HCOO^-$]; **(viii)** the energy consumption per kmol of $HCOO^-$ [EC]; and **(ix)** the standard deviation.

Counter-electrode	Qa/A [mL min^{-1} cm^{-2}]	Absolute cell voltage [V]	Anode potential [V]	[$HCOO^-$] [g L^{-1}]	FE for $HCOO^-$ [%]	r$HCOO^-$ [mmol m^{-2} s^{-1}]	EC [kWh $kmol^{-1}$]	Standard deviation [%]
Pt/C-PE - GOR	0.57	4.95	3.73	89.5	56.1	1.32	467	0.79
Ni-Co/Ni foam - GOR		3.29	2.29	172.5	79.9	1.86	221	3.18
Ni-CMF– GOR (This work)		**3.59**	**2.49**	**74.8**	**63.4**	**1.47**	**305**	**2.98**
Pt/C-PE - GOR	2.28	5.06	3.75	77.4	39.9	0.92	700	2.89
Ni-Co/Ni foam - GOR		3.40	2.39	359.5	95.1	2.21	192	0.98
Ni-CMF – GOR (This work)		**3.66**	**2.68**	**100.1**	**72.9**	**1.69**	**269**	**5.28**

reactions, particularly in alkaline media, thereby providing a means to modify the overall product outcomes.

For this purpose, we developed a MEA-reactor in which the Ni-CMFs were deposited on a carbon cloth substrate, forming the anode, to catalyze the single-pass GOR coupled while the gas-phase CO_2 electroreduction to $HCOO^-$ took place at the cathode. Despite the fact that Ni-CMFs present low metal content compared to Ni-Co/Ni foam-based anodes, the novel MEA-electrolyzer developed proves feasible for the continuous co-valorization of CO_2 and glycerol. Specifically, for an anolyte flow rate and current densities of 2.28 mL min^{-1} cm^{-2} and 45 mA cm^{-2}, respectively, Faradaic efficiencies for LAC and $HCOO^-$ of 20.68 and 38.60 % were obtained, respectively, from glycerol by the employment of Ni-CMF anodes. Simultaneously, highly concentrated $HCOO^-$ solutions of up to 100 g L^{-1}, combined with interesting Faradaic efficiencies of 72.9 %, were obtained at the cathode.

Despite promising results obtained in this study, further research efforts are required to increase the current density without compromising the glycerol product distribution or affecting the cathode performance for $HCOO^-$ production from CO_2.

CRediT authorship contribution statement

Kevin Fernández-Caso: Conceptualization, Methodology, Validation, Investigation, Writing – original draft, Writing – review & editing, Data curation. **Zahra Hagheh-Kavousi:** Methodology, Validation, Investigation, Writing – original draft, Data curation. **Yaovi Holade:** Writing – review & editing, Supervision, Project administration, Funding acquisition. **David Cornu:** Writing – review & editing, Supervision, Project administration, Funding acquisition. **Guillermo Díaz-Sainz:** Conceptualization, Methodology, Investigation, Data curation, Writing – original draft, Writing – review & editing, Supervision. **Manuel Álvarez-Guerra:** Conceptualization, Methodology, Writing – original draft, Writing – review & editing, Supervision, Project administration, Funding acquisition. **Angel Irabien:** Writing – review & editing, Supervision, Project administration, Funding acquisition. **Mikhael Bechelany:** Writing – review & editing, Supervision, Project administration, Funding acquisition

Declaration of competing interest

The authors declare that they have no known competing financial interests or personal relationships that could have appeared to influence the work reported in this paper.

Acknowledgements

The authors gratefully acknowledge financial support through projects PID2019-108136RB-C31 (MCIN/AEI/10.13039/501100011033), PID2022-138491OB-C31 (MICIU/AEI/10.13039/501100011033 and ERDF/EU), TED2021–129810B-C21 (MCIN/AEI/10.13039/501100011033 and European Union Next Generation EU/PRTR), PLEC2022-009398 (MCIN/AEI/10.13039/501100011033 and European Union Next Generation EU/PRTR), PCI2024-155027-2 (MICIU/AEI/10.13039/501100011033/UE) and the "Complementary Plan in the area of Energy and Renewable Hydrogen" funded by Autonomous Community of Cantabria, Spain, and the European Union Next Generation EU/PRTR. The present work is related to CAPTUS Project. This project has received funding from the European Union's Horizon Europe research and innovation programme under grant agreement No 101118265. We are also grateful for the Bi carbon-supported nanoparticles prepared and provided by the group of Prof. V. Montiel and Dr. José Solla-Gullón from the Institute of Electrochemistry of the University of Alicante.

Appendix A. Supplementary data

Supplementary data to this article can be found online at https://doi.org/10.1016/j.jpowsour.2025.236260.

Data availability

No data was used for the research described in the article.

References

[1] F. Yang, M.A. Hanna, R. Sun, Value-added uses for crude glycerol–a byproduct of biodiesel production, Biotechnol. Biofuels 5 (2012) 1–10.
[2] M. Braun, C.S. Santana, A.C. Garcia, C. Andronescu, From waste to value – glycerol electrooxidation for energy conversion and chemical production, Curr. Opin. Green Sustain. Chem. 41 (2023) 100829.
[3] J. Kaur, A.K. Sarma, M.K. Jha, P. Gera, Valorisation of crude glycerol to value-added products: perspectives of process technology, economics and environmental issues, Biotechnol. Report. 27 (2020) e00487.
[4] U.I. Nda-Umar, I. Ramli, Y.H. Taufiq-Yap, E.N. Muhamad, An overview of recent research in the conversion of glycerol into biofuels, fuel additives and other bio-based chemicals, Catalysts 9 (2019) 15.
[5] G. Bagnato, A. Iulianelli, A. Sanna, A. Basile, Glycerol production and transformation: a critical review with particular emphasis on glycerol reforming reaction for producing hydrogen in conventional and membrane reactors, Membranes 7 (2017) 17.
[6] K. Pandit, C. Jeffrey, J. Keogh, M.S. Tiwari, N. Artioli, H.G. Manyar, Techno-economic assessment and sensitivity analysis of glycerol valorization to biofuel additives via esterification, Ind. Eng. Chem. Res. 62 (2023) 9201–9210.
[7] S.B. Costa-Gutierrez, J.M. Saez, J.D. Aparicio, E.E. Raimondo, C.S. Benimeli, M. A. Polti, Glycerol as a substrate for actinobacteria of biotechnological interest: advantages and perspectives in circular economy systems, Chemosphere 279 (2021) 130505.
[8] G. Durnin, J. Clomburg, Z. Yeates, P.J.J. Alvarez, K. Zygourakis, P. Campbell, R. Gonzalez, Understanding and harnessing the microaerobic metabolism of glycerol in Escherichia coli, Biotechnol. Bioeng. 103 (2009) 148–161.
[9] T. Sarchami, E. Johnson, L. Rehmann, Optimization of fermentation condition favoring butanol production from glycerol by Clostridium pasteurianum DSM 525, Bioresour. Technol. 208 (2016) 73–80.
[10] Z.C. Hu, Y.G. Zheng, Y.C. Shen, Use of glycerol for producing 1,3-dihydroxyacetone by Gluconobacter oxydans in an airlift bioreactor, Bioresour. Technol. 102 (2011) 7177–7182.
[11] E.E. Johnson, L. Rehmann, The role of 1,3-propanediol production in fermentation of glycerol by Clostridium pasteurianum, Bioresour. Technol. 209 (2016) 1–7.
[12] G.D. Yadav, R.V. Sharma, S.O. Katole, Selective dehydration of glycerol to acrolein: development of efficient and robust solid acid catalyst MUICaT-5, Ind. Eng. Chem. Res. 52 (2013) 10133–10144.
[13] S. Carrettin, P. McMorn, P. Johnston, K. Griffin, G.J. Hutchings, Selective oxidation of glycerol to glyceric acid using a gold catalyst in aqueous sodium hydroxide, Chem. Commun. 7 (2002) 696–697.
[14] G.M. Lari, G. Pastore, C. Mondelli, J. Pérez-Ramírez, Towards sustainable manufacture of epichlorohydrin from glycerol using hydrotalcite-derived basic oxides, Green Chem. 20 (2018) 148–159.
[15] F. Fantozzi, A. Frassoldati, P. Bartocci, G. Cinti, F. Quagliarini, G. Bidini, E. M. Ranzi, An experimental and kinetic modeling study of glycerol pyrolysis, Appl. Energy 184 (2016) 68–76.
[16] A. Almeida, A. Ribeiro, E. Ramalho, R. Pilão, Crude glycerol gasification in a fixed bed gasifier, Energy Proc. 153 (2018) 149–153.
[17] L. Fan, B. Liu, X. Liu, N. Senthilkumar, G. Wang, Z. Wen, Recent progress in electrocatalytic glycerol oxidation, Energy Technol. 9 (2021) 2000804.
[18] M. Valter, E. Campos, D. Santos, L.G.M. Pettersson, A. Hellman, Partial electrooxidation of glycerol on close-packed transition metal surfaces: insights from first-principles calculations, J. Phys. Chem. C 124 (2020) 17907–17915.
[19] M.S. Ahmad, M.H. Ab Rahim, T.M. Alqahtani, T. Witoon, J.W. Lim, C.K. Cheng, A review on advances in green treatment of glycerol waste with a focus on electro-oxidation pathway, Chemosphere 276 (2021) 130128.
[20] C. Coutanceau, S. Baranton, R.S.B. Kouamé, Selective electrooxidation of glycerol into value-added chemicals: a short overview, Front. Chem. 7 (2019) 1–15.
[21] J. Wu, X. Yang, M. Gong, Recent advances in glycerol valorization via electrooxidation: catalyst, mechanism and device, Chin. J. Catal. 43 (2022) 2966–2986.
[22] K. Fernández-Caso, G. Díaz-Sainz, M. Alvarez-Guerra, A. Irabien, Electroreduction of CO_2: advances in the continuous production of formic acid and formate, ACS Energy Lett. 8 (2023) 1992–2024.
[23] G. Díaz-Sainz, K. Fernández-Caso, T. Lagarteira, S. Delgado, M. Alvarez-Guerra, A. Mendes, A. Irabien, Coupling continuous CO_2 electroreduction to formate with efficient Ni-based anodes, J. Environ. Chem. Eng. 11 (2023) 109171.
[24] Y. Zhang, Y. Chen, R. Liu, X. Wang, H. Liu, Y. Zhu, Q. Qian, Y. Feng, M. Cheng, G. Zhang, Oxygen vacancy stabilized $Bi_2O_2CO_3$ nanosheet for CO_2 electroreduction at low overpotential enables energy efficient CO-production of formate, InfoMat 5 (2023) e12375.
[25] X. Liu, K. Zhang, Y. Sun, S. Zhang, Z. Qiu, T. Song, J. Xie, Y. Wu, Y. Chen, Upgrading CO_2 into acetate on Bi_2O_3@carbon felt integrated electrode via coupling electrocatalysis with microbial synthesis, SusMat 3 (2022) 235–247.
[26] Y. Zhang, Y. Chen, X. Wang, Y. Feng, H. Zhang, G. Zhang, Self-polarization triggered multiple polar units toward electrochemical reduction of CO_2 to ethanol with high selectivity, Angew. Chem. Int. Ed. 62 (2023) e202302241.
[27] I. Dutta, S. Chatterjee, H. Cheng, R.K. Parsapur, Z. Liu, Z. Li, E. Ye, H. Kawanami, J. S.C. Low, Z. Lai, X.J. Loh, K.W. Huang, Formic acid to power towards low-carbon economy, Adv. Energy Mater. 2103799 (2022) 1–17.
[28] H. Yang, J.J. Kaczur, S.D. Sajjad, R.I. Masel, Performance and long-term stability of CO_2 conversion to formic acid using a three-compartment electrolyzer design, J. CO_2 Util. 42 (2020) 101349.
[29] H. Yang, J.J. Kaczur, S.D. Sajjad, R.I. Masel, Electrochemical conversion of CO_2 to formic acid utilizing SustainionTM membranes, J. CO_2 Util. 20 (2017) 208–217.
[30] L. Li, A. Ozden, S. Guo, F. Pelayo García de Arquer, C. Wang, M. Zhang, J. Zhang, H. Jiang, W. Wang, H. Dong, D. Sinton, E.H. Sargent, M. Zhong, Stable, active CO_2 reduction to formate via redox-modulated stabilization of active sites, Nat. Commun. 12 (2021) 5223.
[31] L. Fan, C. Xia, P. Zhu, Y. Lu, H. Wang, Electrochemical CO_2 reduction to high-concentration pure formic acid solutions in an all-solid-state reactor, Nat. Commun. 11 (2020) 3633.
[32] C. Xia, P. Zhu, Q. Jiang, Y. Pan, W. Liang, E. Stavitsk, H.N. Alshareef, H. Wang, Continuous production of pure liquid fuel solutions via electrocatalytic CO_2 reduction using solid-electrolyte devices, Nat. Energy 4 (2019) 776–785.
[33] G. Díaz-Sainz, M. Alvarez-Guerra, B. Ávila-Bolívar, J. Solla-Gullón, V. Montiel, A. Irabien, Improving trade-offs in the figures of merit of gas-phase single-pass continuous CO_2 electrocatalytic reduction to formate, Chem. Eng. J. 405 (2021) 126965.
[34] W. Fang, W. Guo, R. Lu, Y. Yan, X. Liu, D. Wu, F.M. Li, Y. Zhou, C. He, C. Xia, H. Niu, S. Wang, Y. Liu, Y. Mao, C. Zhang, B. You, Y. Pang, L. Duan, X. Yang, F. Song, T. Zhai, G. Wang, X. Guo, B. Tan, T. Yao, Z. Wang, B.Y. Xia, Durable CO_2 conversion in the proton-exchange membrane system, Nature 626 (2024) 86–91.
[35] L. Lin, X. He, X.G. Zhang, W. Ma, B. Zhang, D. Wei, S. Xie, Q. Zhang, X. Yi, Y. Wang, A nanocomposite of bismuth clusters and $Bi_2O_2CO_3$ sheets for highly efficient electrocatalytic reduction of CO_2 to formate, Angew. Chem. Int. Ed. 62 (2023) e202214959.
[36] W. Lee, Y.E. Kim, M.H. Youn, S.K. Jeong, K.T. Park, Catholyte-free electrocatalytic CO_2 reduction to formate, Angew. Chem. Int. Ed. 130 (2018) 6999–7003.
[37] B. De Mot, M. Ramdin, J. Hereijgers, T.J.H. Vlugt, T. Breugelmans, Direct water injection in catholyte-free zero-gap carbon dioxide electrolyzers, Chemelectrochem 7 (2020) 3839–3843.
[38] Z. Zhang, X. Huang, Z. Chen, J. Zhu, B. Endrődi, C. Janáky, D. Deng, Membrane electrode assembly for electrocatalytic CO_2 reduction: principle and application, Angew. Chem. Int. Ed. 62 (2023) e202302789.
[39] A.C. Garcia, M.J. Kolb, C. Van Nierop Y Sanchez, J. Vos, Y.Y. Birdja, Y. Kwon, G. Tremiliosi-Filho, M.T.M. Koper, Strong impact of platinum surface structure on primary and secondary alcohol oxidation during electro-oxidation of glycerol, ACS Catal. 6 (2016) 4491–4500.
[40] Y. Liu, W. Yu, D. Raciti, D.H. Gracias, C. Wang, Electrocatalytic oxidation of glycerol on platinum, J. Phys. Chem. C 123 (2019) 426–432.
[41] M. Valter, M. Busch, B. Wickman, H. Grönbeck, J. Baltrusaitis, A. Hellman, Electrooxidation of glycerol on gold in acidic medium: a combined experimental and dft study, J. Phys. Chem. C 122 (2018) 10489–10494.
[42] H. Mou, F. Lu, Z. Zhuang, Q. Chang, L. Zhang, X. Chen, Y. Zhang, J.G. Chen, Glycerol electrooxidation over precision-synthesized gold nanocrystals with different surface facets, Precis. Chem. 2 (2024) 103–111.
[43] I. Terekhina, J. White, A. Cornell, M. Johnsson, Electrocatalytic oxidation of glycerol to value-added compounds on Pd nanocrystals, ACS Appl. Nano Mater. 6 (2023) 11211–11220.
[44] M. Weber, P. Collot, H. El Gaddari, S. Tingry, M. Bechelany, Y. Holade, Enhanced catalytic glycerol oxidation activity enabled by activated-carbon-supported palladium catalysts prepared through atomic layer deposition, Chemelectrochem 5 (2018) 743–747.
[45] T. Li, D.A. Harrington, An overview of glycerol electrooxidation mechanisms on Pt, Pd and Au, ChemSusChem 14 (2021) 1472–1495.
[46] C. Xu, Y. Hu, J. Rong, S.P. Jiang, Y. Liu, Ni hollow spheres as catalysts for methanol and ethanol electrooxidation, Electrochem. Commun. 9 (2007) 2009–2012.
[47] T. Maiyalagan, K. Scott, Performance of carbon nanofiber supported Pd-Ni catalysts for electro-oxidation of ethanol in alkaline medium, J. Power Sources 195 (2010) 5246–5251.
[48] G. Wang, J. Chen, K. Li, J. Huang, Y. Huang, Y. Liu, X. Hu, B. Zhao, L. Yi, T. W. Jones, Z. Wen, Cost-effective and durable electrocatalysts for Co-electrolysis of CO_2 conversion and glycerol upgrading, Nano Energy 92 (2022) 106751.
[49] M.S.E. Houache, R. Safari, U.O. Nwabara, T. Rafaïdeen, G.A. Botton, P.J.A. Kenis, S. Ve Baranton, C. Coutanceau, E.A. Baranova, Selective electrooxidation of glycerol to formic acid over carbon supported Ni1−x mx (M = Bi, Pd, and Au) nanocatalysts and coelectrolysis of CO_2, ACS Appl. Energy Mater. 3 (9) (2020) 8725–8738.
[50] A. Kormányos, A. Szirmai, B. Endrődi, C. Janáky, Stable operation of paired CO_2 reduction/glycerol oxidation at high current density, ACS Catal. 14 (2024) 6503–6512.
[51] A. Balog, E. Kecsenovity, G.F. Samu, J. He, D. Fekete, C. Janáky, Paired photoelectrochemical conversion of CO_2/H_2O and glycerol at high rate, Catal 7 (2024) 522–535.
[52] M.A. Khan, S.K. Nabil, T. Al-Attas, N.G. Yasri, S. Roy, M.M. Rahman, S. Larter, P. M. Ajayan, J. Hu, M.G. Kibria, Zero-crossover electrochemical CO_2 reduction to

ethylene with co-production of valuable chemicals, Chem Catal. 2 (8) (2022) 2077–2095.
[53] Y. Pei, Z. Pi, H. Zhong, J. Chenga, F. Jin, Glycerol oxidation-assisted electrochemical CO_2 reduction for the dual production of formate, J. Mater. Chem. 10 (2022) 1309–1319.
[54] X. Guo, S.-M. Xu, H. Zhou, Y. Ren, R. Ge, M. Xu, L. Zheng, X. Kong, M. Shao, Z. Li, H. Duan, Engineering hydrogen generation sites to promote electrocatalytic CO_2 reduction to formate, ACS Catal. 12 (2022) 10551–10559.
[55] K. Fernández-Caso, A. Peña-Rodríguez, J. Solla-Gullón, V. Montiel, G. Díaz-Sainz, M. Alvarez-Guerra, A. Irabien, Continuous carbon dioxide electroreduction to formate coupled with the single-pass glycerol oxidation to high value-added products, J. CO_2 Util. 70 (2023) 102431.
[56] J. Vehrenberg, J. Baessler, A. Decker, R. Keller, Paired electrochemical synthesis of formate via oxidation of glycerol and reduction of CO_2 in a flow cell reactor, Electrochem. Commun. (2023) 107497.
[57] A. Peña, K. Fernández-Caso, G. Diaz-Sainz, M. Alvarez-Guerra, V. Montiel, J. Solla-Gullon, Single-pass electrooxidation of glycerol on bismuth-modified platinum electrodes as an anodic process coupled to the continuous CO_2 electroreduction toward formate, ACS Sustain. Chem. Eng. 12 (2024) 3671–3679.
[58] A.J.R.C. Junqueira, D. Das, A.C. Brix, S. Dieckhöfer, J. Weidner, X. Wang, J. Shi, Simultaneous anodic and cathodic formate production in a paired electrolyzer by CO_2 reduction and glycerol oxidation, ChemSusChem 16 (2023) e202202349.
[59] B. van den Bosch, B. Rawls, M.B. Brands, C. Koopman, M.F. Phillips, M. C. Figueiredo, G.J.M. Gruter, Formate over-oxidation limits industrialization of glycerol oxidation paired with carbon dioxide reduction to formate, ChemPlusChem 88 (2023) e202300112.
[60] K. Fernández-Caso, M. Molera, T. Andreu, J. Solla-Gullón, V. Montiel, G. Díaz-Sainz, M. Álvarez-Guerra, A. Irabien, Coupling glycerol oxidation reaction using Ni-Co foam anodes to CO_2 electroreduction in gas-phase for continuous co-valorization, Chem. Eng. J. 480 (2024) 147908.
[61] B. You, N. Jiang, M. Sheng, M.W. Bhushan, Y. Sun, Hierarchically porous urchin-like Ni_2P superstructures supported on nickel foam as efficient bifunctional electrocatalysts for overall water splitting, ACS Catal. 6 (2016) 714–721.
[62] X. Lu, C. Zhao, Electrodeposition of hierarchically structured three-dimensional nickel-iron electrodes for efficient oxygen evolution at high current densities, Nat. Commun. 6 (2015) 6616.
[63] P. Zhang, L. Li, D. Nordlund, H. Chen, L. Fan, B. Zhang, X. Sheng, Q. Daniel, L. Sun, Dendritic core-shell nickel-iron-copper metal/metal oxide electrode for efficient electrocatalytic water oxidation, Nat. Commun. 9 (2018) 1–10.
[64] R. Iwata, L. Zhang, K.L. Wilke, S. Gong, M. He, B.M. Gallant, E.N. Wang, Bubble growth and departure modes on wettable/non-wettable porous foams in alkaline water splitting, Joule 5 (2021) 887–900.
[65] P. Serp, M. Corrias, P. Kalck, Carbon nanotubes and nanofibers in catalysis, Appl. Catal. Gen. 253 (2003) 337–358.
[66] A. Barhoum, R. Rasouli, M. Yousefzadeh, H. Rahier, M. Bechelany, Nanofiber Technology: History and Developments, Handbook of Nanofibers, Springer Nature, 2018.
[67] A. Barhoum, K. Pal, H. Rahier, H. Uludag, I.S. Kim, M. Bechelany, Nanofibers as new-generation materials: from spinning and nano-spinning fabrication techniques to emerging applications, Appl. Mater. Today 17 (2019) 1–35.
[68] M. Weber, N. Tuleushova, J. Zgheib, C. Lamboux, I. Iatsunskyi, E. Coy, V. Flaud, S. Tingry, D. Cornu, P. Miele, M. Bechelany, Y. Holade, Enhanced electrocatalytic performance triggered by atomically bridged boron nitride between palladium nanoparticles and carbon fibers in gas-diffusion electrodes, Appl. Catal. B Environ. 257 (2019) 117917.
[69] R.D. Castranova V, P.A. Schulte, Zumwalde, Carbon nanotubes and carbon nanofibers, Acc. Chem. Res. 46 (2013) 642–649.
[70] M. Zhang, R. Nie, L. Wang, J. Shi, W. Du, Z. Hou, Selective oxidation of glycerol over carbon nanofibers supported Pt catalysts in a base-free aqueous solution, Catal. Commun. 59 (2015) 5–9.
[71] K.P. De Jong, J.W. Geus, Carbon nanofibers: catalytic synthesis and applications, Catal. Rev. - Sci. Eng. 42 (2000) 481–510.
[72] B. Ávila-Bolívar, L. García-Cruz, V. Montiel, J. Solla-Gullón, Electrochemical reduction of CO_2 to formate on easily prepared carbon-supported Bi nanoparticles, Molecules 24 (2019) 2032.
[73] W. Tang, Z. Chen, M. Millan, X. Zuo, G. Yuan, Z. Cui, Z. Dong, Y. Cong, X. Li, Facile fabrication of porous carbon nanofibers encapsulated with nanoscale exposed Ni for producing high-purity hydrogen from cheap glycerol, Int. J. Hydrogen Energy 48 (2023) 38172–38187.
[74] J.T. Richardson, R. Scates, M.V. Twigg, X-ray diffraction study of nickel oxide reduction by hydrogen, Appl. Catal. Gen. 246 (2003) 137–150.
[75] V.L. Oliveira, C. Morais, K. Servat, T.W. Napporn, G. Tremiliosi-Filho, K.B. Kokoh, Studies of the reaction products resulted from glycerol electrooxidation on Ni-based materials in alkaline medium, Electrochim. Acta 117 (2014) 255–262.
[76] V.L. Oliveira, C. Morais, K. Servat, T.W. Napporn, G. Tremiliosi-Filho, K.B. Kokoh, Glycerol oxidation on nickel based nanocatalysts in alkaline medium - identification of the reaction products, J. Electroanal. Chem. 703 (2013) 56–62.
[77] A. Medrano-Banda, E. Ginoux, T. Faverge, A. Oshchepkov, A. Bonnefont, M. Chatenet, C. Coutanceau, G. Kéranguéven, P. Cognet, E. Savinova, Electrochemical oxidation of glucose in alkaline environment—a comparative study of Ni and Au electrodes, Electrochim. Acta 487 (2024) 144159.
[78] M.S.E. Houache, E. Cossar, S. Ntais, E.A. Baranova, Electrochemical modification of nickel surfaces for efficient glycerol electrooxidation, J. Power Sources 375 (2018) 310–319.
[79] T. Andreu, M. Mallafré, M. Molera, M. Sarret, R. Oriol, I. Sirés, Effect of thermal treatment on nickel-cobalt electrocatalysts for glycerol oxidation, Chemelectrochem 9 (2022) 1–7.
[80] V.L. Oliveira, C. Morais, K. Servat, T.W. Napporn, G. Tremiliosi-Filho, K.B. Kokoh, Studies of the reaction products resulted from glycerol electrooxidation on Ni-based materials in alkaline medium, Electrochim. Acta 117 (2014) 255–262.
[81] J. Resasco, L.D. Chen, E. Clark, C. Tsai, C. Hahn, T.F. Jaramillo, K. Chan, A.T. Bell, Promoter effects of alkali metal cations on the electrochemical reduction of carbon dioxide, J. Am. Chem. Soc. 139 (2017) 11277–11287.